Tribol Lett (2014) 53:255–260
DOI 10.1007/s11249-013-0263-2

ORIGINAL PAPER

Transient Characteristics of Nanoscale Air Bearings Subjected to Joule Heating

Jia-Yang Juang

Received: 11 July 2013 / Accepted: 31 October 2013 / Published online: 9 November 2013

Abstract Transient characteristic of heat exchange between closely positioned bodies has become an important issue owing to the continuous miniaturization of many technologies such as high-density magnetic recording, integrated circuits, and atomic force microscopy. We experimentally and numerically study the transient characteristics of nanoscale air bearings subjected to Joule heating of a nearby heating element in hard disk drives. Our results reveal that the response consists of multiple characteristic times, and at least two terms ($\tau_1 = 162$ μs and $\tau_2 = 23$ μs) are required to capture the transient response. We present a one-dimensional analytical model that provides a better understanding of the nature of the transient characteristics and an efficient way to obtain their trends and bounds. Our model may also explain the much faster response due to laser heating observed in heat-assisted magnetic recording system.

Keywords Air-bearing sliders · Head–disk interface · Thermal flying height control · Heat-assisted magnetic recording

1 Introduction

The rise of "big data," the idea that the world is replete with more information and much more information is put to extraordinary new uses than ever, has changed the way we think about the world. Today, there is an estimated 1,200 exabytes' worth of information, and more than 98 % of all stored information is digital [1]. Magnetic recording accounts for a significant portion. Areal density of magnetic recording has increased dramatically since the launch of commercial hard disk drives in the 1950s. Along with advances in heads, media, signal processing, and servo technology, areal density growth is enabled by continuous reduction in head-media spacing (HMS), which comprises of flying height (FH), head and disk protective carbon overcoats, and disk lubricant. Current products have HMS on the order of 10 nm, corresponding to an areal density of 500 Gb/in^2, and the HMS includes an FH of 5 nm, overcoats on the head and disk of 2 nm each, and about 1 nm of disk lubricant [2]. Reduction in FH and minimization of FH modulation are critical to the capacity and performance [3]. The FH, pitch, and roll of a slider are determined by a meticulously designed and fabricated patterned surface, known as air-bearing surface (ABS), on the bottom surface of the slider which generates a nanoscale air bearing, allowing the slider to fly on a spinning disk. The FH of such "self-acting" air bearings has been decreased from over 300 nm in 1981 to several nanometers today [4]. Those air bearings are passive, meaning that once the slider is fabricated and assembled into a drive its FH is not adjustable and is subjected to environmental changes such as altitude, temperature, and humidity. Besides, head-to-head variation due to manufacturing tolerance accounts for a considerable portion of the FH budget. Moreover, FH was found to modulate even when a slider flies at a given radial position mainly due to disk "run-out" caused by clamping [5]. Considerable FH modulation combined with short range attractive forces, such as intermolecular, electrostatic and meniscus forces, may cause instability of the head–disk interface. An alternative to lowering FH and minimizing its modulation is to integrate an actuator in the head and to actively control the FH [6]. Yeack-Scranton

J.-Y. Juang (✉)
Department of Mechanical Engineering, National Taiwan University, Taipei 10617, Taiwan
e-mail: jiayang@ntu.edu.tw

et al. [7] first proposed an active slider with an integrated piezoelectric bender and demonstrated that the FH was reduced from ~200 nm to contact. Juang and Bogy [8, 9] later proposed a nonlinear compensator design using piezoelectric actuation to dynamically suppress the modulation. However, integrating piezoelectric materials in the slider presents a formidable challenge in the fabrication process and may be difficult to implement in mass production [10, 11].

Another approach using Joule heating for FH control, known as thermal flying height control (TFC), was recently introduced and successfully implemented in most of today's HDDs [6, 12–14]. In a TFC slider, a microscale resistive heating element (heater) is deposited near the TMR sensor (reader) and write pole (writer). Localized internal heat source is created by passing an electrical current through the heater, and the slider expands due to mismatch of the coefficients of thermal expansion of the various materials and a nonuniform temperature distribution, causing the reader and writer to protrude below the ABS plane, hence, reducing the FH. TFC allows for calibrating the FH of individual heads by a "touchdown and pull-back" scheme, in which the power is gradually increased until the head–disk contact is detected, and then the protruded bulge is "pulled back" by reducing the power by a certain amount to achieve a desirable FH for reading and writing [14]. The head-media spacing can be estimated by Wallace spacing loss equation based on read-back signal strength [15]. Head-to-head FH variation due to manufacturing tolerances can be minimized. Such an operation is only in a "static sense", i.e., the power level is preset when a HDD assembled, and is independent of the circumferential position of the slider over the disk. A smooth transition between reading, writing, and idle condition is not considered.

Boettcher et al. [16] proposed a feedforward control algorithm to dynamically adjust the heater power so that the FH modulation is reduced. Also, at sub-2 nm regime the transient response of FH becomes critical, in particular at the transition of reading, writing, and idle conditions. A harmful head–disk contact can occur at transition if the transient response is not considered. Despite the great interest, a complete understanding of the nature of the characteristic times of nanoscale air bearings subjected to Joule heating is still lacking.

In this letter, we study the transient characteristics of TFC slider subjected to Joule heating. We measure flying height modulation using drive-level read-back signal and numerically simulate transient responses of flying height, temperature, and protrusion by an integrated air-bearing/finite-element model (FEM). We present a simple analytical model to understand the nature of the transient characteristics.

2 Analytical Models

Without loss of generosity, we study the nanoscale air bearing generated in the head–disk interface (HDI) when a femto slider (850 μm × 700 μm × 230 μm) flies over a spinning disk, as shown schematically in Fig. 1. The disk rotational speed is 5,400 rpm, i.e. 12.5 m/s at a radius of 22 mm, and the air-bearing surface is a production design with three etching steps. The magnetic head is fabricated on an Al_2O_3–TiC substrate. The head has a 3-turn helix coil and a bottom pole (P1) thickness of 1.2 μm. The top and bottom shields (S1, S2) are both 1 μm thick. The distance between the TMR sensor and the write pole is 6.5 μm. The heater is located between the substrate and S1 and is embedded in the overcoat along with the shields and poles. The overcoat is made of Al_2O_3 which has a low thermal conductivity of 1.5 W/m K and, hence, serves as thermal insulation.

The general three-dimensional (3D) heat conduction equation is

$$\frac{\partial}{\partial x}\left(k\frac{\partial T}{\partial x}\right)+\frac{\partial}{\partial y}\left(k\frac{\partial T}{\partial y}\right)+\frac{\partial}{\partial z}\left(k\frac{\partial T}{\partial z}\right)+\dot{q}=\rho c\frac{\partial T}{\partial t} \qquad (1)$$

where k, ρ, and c are the thermal conductivity, density, and specific heat of the head materials, respectively. $\dot{q}$ is the heat generated per unit volume by the heater. For constant thermal conductivity, Eq. (1) is written

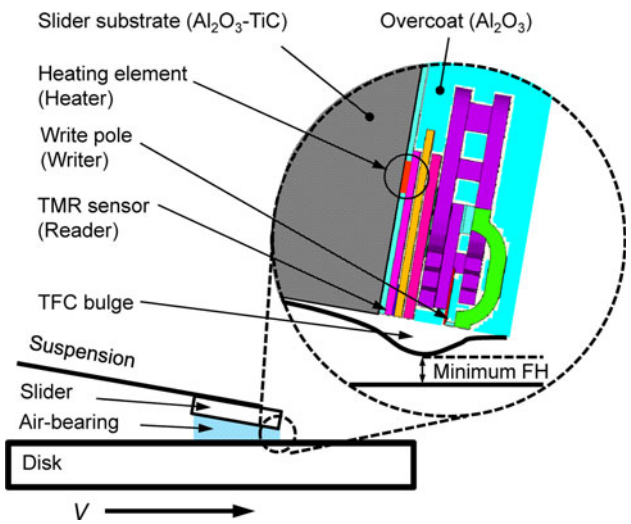

Fig. 1 Schematic of head–disk interface and cross-section of a protruded TFC slider flying over a spinning disk at a linear velocity V. The heater element (heater), TMR sensor (reader), and write pole (writer) are located near the trailing edge of the slider. An air-bearing film is generated between the slider and disk. The minimum FH is ~1 nm and the FH near the leading edge is ~100 nm; pitch: 120 μrad, roll: 3 μrad. The TFC bulge is generated due to Joule heating of the heater. The slider form factor is of femto size (850 μm × 700 μm × 230 μm), and its minimum FH is ~10 nm when no power is applied to the heater

$$\frac{\partial^2 T}{\partial x^2}+\frac{\partial^2 T}{\partial y^2}+\frac{\partial^2 T}{\partial z^2}+\frac{\dot{q}}{k}=\frac{1}{D}\frac{\partial T}{\partial t} \tag{2}$$

where $D = k/\rho c$ is the thermal diffusivity of the material. The larger the value of D, the faster heat diffuses through the material.

At the head–disk interface, the heat flux across the air bearing can be expressed as [12]

$$\begin{aligned} q''(x,y) &= -q''_{\text{conduction}} + q''_{\text{viscous}} \\ &= -k_{\text{air}}\frac{T_s(x,y)-T_d}{FH(x,y)+2b\lambda(x,y)} + q''_{\text{viscous}} \end{aligned} \tag{3}$$

where x and y are the rectangular coordinates of the slider, T_s and T_d are the temperature of the slider and disk, respectively, k_{air} is the thermal conductivity of air, FH is the flying height or slider-disk spacing, λ is the mean free path of air, $b = 2(2-\sigma_T)\gamma/\sigma_T(\gamma+1)Pr$, σ_T is the thermal accommodation coefficient, γ is the ratio of the specific heat, and Pr is the Prandtl number. The heat flux due to viscous dissipation q''_{viscous}, which transfers heat from the air bearing to the slider, is about one to two orders of magnitude smaller than the heat conduction $q''_{\text{conduction}}$ when the temperature difference across the HDI is not close to zero and can be ignored. The interface thermal conductance coefficient across air bearing, $h = k_{\text{air}}/\text{FH}(x,y) + 2b\lambda(x,y)$, is a strong function of both FH and air-bearing pressure and has a peak value ranging from 1 to 2 MW/m^2 K for a typical commercial ABS design. The heat transfer coefficient on the other five surfaces of the slider is on the order of 100 W/m^2 K, which is 3–4 orders of magnitude smaller than that of the ABS. Those surfaces, hence, can be considered as adiabatic, and almost all the heat generated by the heater losses through the air bearing.

Equations (1) and (3), in principal, can be used to solve transient heat transfer problems with internal heat source such as TFC and heat-assisted magnetic recording (HAMR). Solving coupled thermoelastic constitutive equations yields both temperature and displacement fields within the slider. The air-bearing attitude of the protruded slider can then be solved by the generalized Reynolds equation:

$$\begin{aligned} &\frac{\partial}{\partial X}\left[\hat{Q}PH^3\frac{\partial P}{\partial X}-\Lambda_x PH\right]+\frac{\partial}{\partial Y}\left[\hat{Q}PH^3\frac{\partial P}{\partial Y}-\Lambda_y PH\right] \\ &\quad=\sigma\frac{\partial}{\partial T}[PH] \end{aligned} \tag{4}$$

where $X = x/L$, $Y = y/L$, x and y are the distances along the slider's length and width directions, respectively, L is the slider's length, $P = p/p_a$, p is the air-bearing pressure, p_a is the ambient air pressure, $H = \text{FH}/\text{FH}_m$, FH_m is a reference flying height, $T = \omega t$, t is time, ω is the disk's angular frequency, $\Lambda_x = 6\mu U_x L/p_a \text{FH}_m^2$ and $\Lambda_y = 6\mu U_y L/p_a \text{FH}_m^2$ are the bearing numbers in the x and y directions, respectively, $\sigma = 12\mu\omega L^2/p_a FH_m^2$ is the squeeze number, $\hat{Q}$ is the dimensionless mass flow rate of the Poiseuille flow.

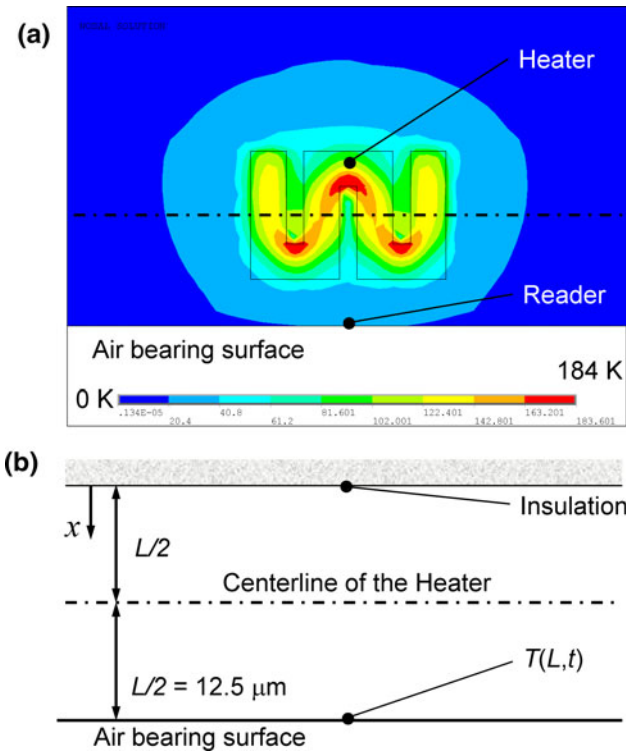

Fig. 2 **a** Simulated temperature distribution at 2 ms near the heater when a 80-mW step power is applied to the heater. The surrounding material is Al_2O_3. **b** A simple 1D analytical model used to derive *upper* and *lower* bounds of the characteristic times

However, the complex structure and materials of the head prevent us from obtaining an exact analytical solution. Numerical approaches are widely used in practice, and predictions of steady-state results are in good agreement with measurements [13]. For transient responses, numerical simulations are usually time-consuming and are limited to provide insights into the nature of the characteristic times.

Even though the exact analytical solution does not exist, we may obtain analytical expressions of the upper and lower bounds of the characteristic times by approximating the original heat transfer problem near the heater to a simple one-dimensional (1D) plane wall with heat loss to the air bearing. We apply 80 mW to the heater and examine the temperature distribution at 2 ms as shown in Fig. 2a. We find that the region of elevated temperature is confined within approximately twice the distance between the ABS and the center of the heater due to the extremely low thermal conductive oxide and the extremely effective air-bearing cooling. It is reasonable to assume that conduction occurs exclusively in the x-direction. Consider the simple one-dimensional plane wall model as shown in Fig. 2b. The surface at $x = 0$ is adiabatic, and the surface

at $x = L$ is subjected to a convective condition corresponding to a coefficient of h. If the wall is initially at a uniform temperature, $T(x, 0) = T_i$, and suddenly immersed in a fluid of $T_\infty \neq T_i$, an exact solution is of the form [17]

$$\frac{T - T_\infty}{T_i - T_\infty} \equiv \frac{\theta}{\theta_i} \equiv \theta^* = \sum_{n=1}^{\infty} C_n \exp\left(-\xi_n^2 F_o\right) \cos(\varsigma_n x^*) \quad (5)$$

where $x^* \equiv x/L$, L is the thickness of the plane wall, the Fourier number $Fo = Dt/L^2$, the coefficient C_n is

$$C_n = \frac{4 \sin \xi_n}{2\xi_n + \sin(2\xi_n)} \quad (6)$$

and the discrete values of ζ_n are positive roots of the transcendental equation

$$\xi_n \tan \xi_n = Bi \quad (7)$$

where $Bi \equiv hL/k$ is the Biot number, k is the thermal conductive of the wall, and h is the air-bearing interface thermal conductance coefficient in Eq. (3).

It is noted that Eq. (5) reveals that the solution for the dimensionless temperature rise is in the form of an infinite series with the time variable t in the exponents of the exponential functions. Except for very small values of the Fourier number, this series may be approximated by the first several terms. The characteristic times may now be obtained as

$$t_n = \frac{L^2}{\xi_n^2 D} = \frac{L^2 \rho c}{\xi_n^2 k} \quad (8)$$

To reduce the characteristic times, and hence increase the actuation bandwidth, one may increase the thermal diffusivity of the material surrounding the heater, reduce the distance of the heater to the ABS, and increase the interface thermal conductance of the air bearing. In practice, the material properties k, ρ, and c of a magnetic head are coordinate-dependent, and the wall is heated when a step power is applied to the embedded heater. However, upper and lower bounds of the characteristic times may be obtained by assuming the head is made of Al_2O_3 overcoat ($k = 1.5$ W/m K, $\rho = 3{,}900$ kg/m^3, $c = 670$ J/kg K) and Al_2O_3–TiC substrate ($k = 24.8$ W/m K, $\rho = 4{,}200$ kg/m^3, $c = 800$ J/kg K), respectively. The interface thermal conductance is not uniform on the ABS, and its maximum is located very close to the reader and writer. We use a constant $h = 1.5$ MW/m^2 K for both cases and obtain a Biot number of 25 and 1.5 for Al_2O_3 and Al_2O_3–TiC, respectively. Accordingly we have the upper bounds of the first two characteristic times $\tau_1 = 477$ μs and $\tau_2 = 53$ μs, and the lower bounds $\tau_1 = 86$ μs and $\tau_2 = 7$ μs. Note that the ratios of the slow and fast times are 9 and 12 for the upper and lower bound cases, respectively.

3 Experimental Measurements and Numerical Simulations

We conduct drive-level flying height measurement based on read-back signal from data sectors on the disks of a 2.5" mobile drive. The measurements are performed at a radius of 22 mm, a skew angle of 0.881 degree, a rotational speed of 5,400 rpm, and a linear velocity of 12.4 m/s. We calculate the flying height change induced by the thermal actuation by applying the Wallace spacing formula as follows [15]

$$\Delta \mathrm{FH} = \frac{\lambda}{2\pi} \ln\left(\frac{A_1}{A_2}\right) \quad (9)$$

where λ is the written wavelength and A_1/A_2 is the amplitude ratio of the read-back signal. We typically use short wavelengths (50–100 nm) for higher resolutions.

Representative transient FH changes subjected to the step Joule heating and removal of the heating (cooling) are shown in Fig. 3a, b, respectively. We find that at least two exponential terms are required to fit the measured data pointed. The characteristic times are determined to be

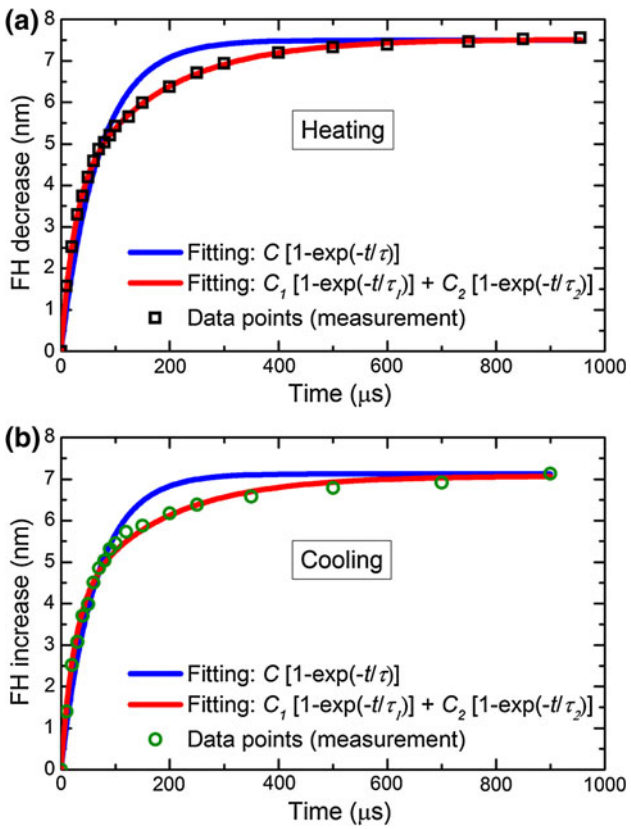

Fig. 3 Representative flying height changes measured by read-back signal. Heating power is 100 mW. **a** Heating: $C_1 = 3.89$, $C_2 = 3.63$, $\tau_1 = 161.94$ μs, $\tau_2 = 23.43$ μs, $C = 7.5$, $\tau = 69.29$ μs; **b** cooling: $C_1 = 3.82$, $C_2 = 3.26$, $\tau_1 = 161.94$ μs, $\tau_2 = 23.43$ μs, $C = 7.13$, $\tau = 63$ μs

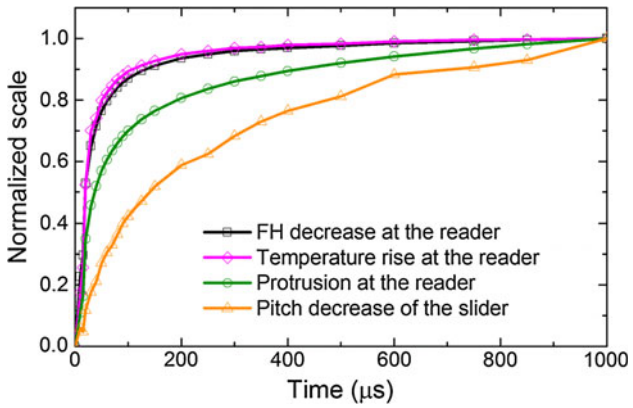

Fig. 4 Simulated transient responses at the reader, FH decrease, reader temperature rise, protrusion, and pitch

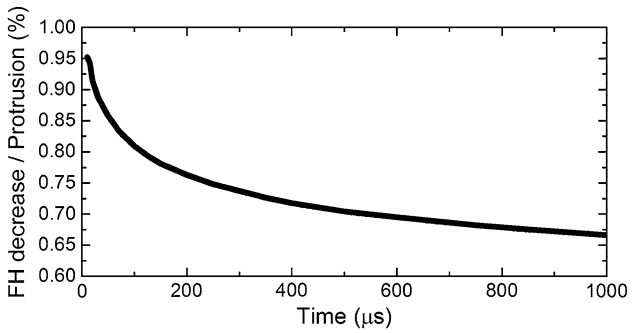

Fig. 5 The ratio of the FH decrease to the protrusion reduces over time, indicating that the air-bearing "push-back effect" is more pronounced when the FH is smaller. At the beginning of heating, the push-back effect is small and most of the protrusion turns into the FH reduction, causing the FH to reach the steady-states much faster than the protrusion

$\tau_1 = 161.94$ μs and $\tau_2 = 23.4$ μs for both heating and cooling processes. The transient characteristics are identical in heating and cooling, though their responses may appear different due to different initial conditions. Both values are within the upper and lower bounds derived in our simple analytical models.

We carry out transient electrical–thermal–structural simulations using a three-dimensional finite-element model (FEM) of the entire slider with detailed head structures and the boundary condition on the ABS derived in Eq. (3). The heat generation due to Joule heating is calculated based on current density within the heater of which one end is grounded and the other applied a constant voltage. Simulated results of FH decrease, temperature rise, protrusion at the reader, and pitch decrease in the slider are normalized and shown in Fig. 4. FH, temperature and protrusion are local parameters, whereas pitch decrease is a global parameter. From Fig. 4, we observe that (1) the FH and temperature at the reader reach steady-states much faster than the protrusion and pitch, (2) the FH follows the temperature rise well owing to adaptive nature of the air bearing, (3) pitch decrease is very

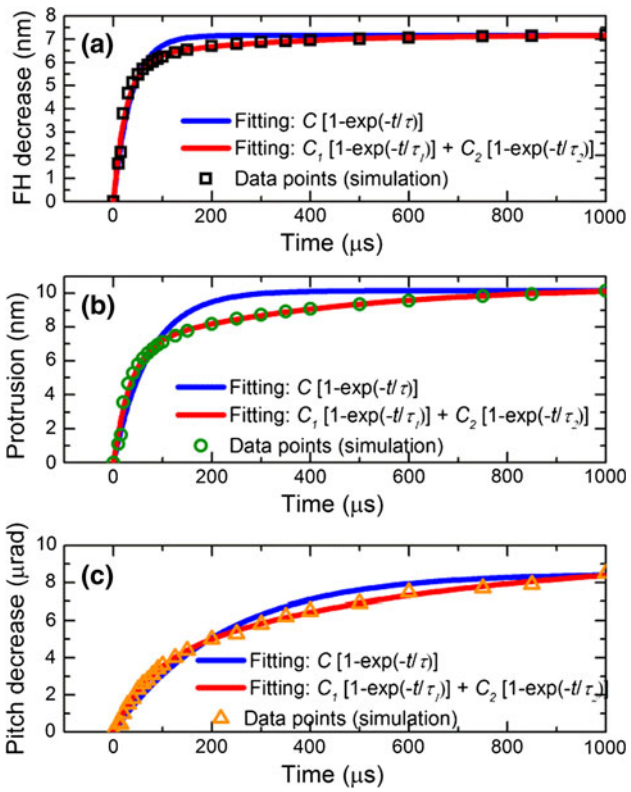

Fig. 6 Simulation data points and curve fittings of **a** FH decreases ($\tau_1 = 257$ μs, $\tau_2 = 26$ μs), **b** protrusion ($\tau_1 = 420$ μs, $\tau_2 = 35$ μs), and **c** pitch decrease ($\tau_1 = 614$ μs, $\tau_2 = 76$ μs) with a 80-mW heating power

slow since it requires a steady-state of the entire slider instead of the local heated region near the heater, and (4) the FH at the reader reaches the steady-states much faster than the protrusion. As shown in Fig. 5, the ratio of the FH decrease to the protrusion reduces over time, indicating that the air-bearing "push-back effect" is more pronounced when the FH is smaller. At the beginning of heating, the push-back effect is small and most of the protrusion turns into the FH reduction, causing the FH to reach the steady-states much faster than the protrusion.

To obtain the characteristics times, we fit the simulation data with a series of exponential functions. We find that at least two terms are required to obtain satisfactory fittings for the FH, protrusion, and pitch decrease as shown in Fig. 6. The characteristic times of the FH are $\tau_1 = 257.5$ μs and $\tau_2 = 25.7$ μs and are in reasonably good agreement with our measurements.

The characteristic times are proportional to L^2 and approximately inversely proportional to k according to Eq. (8). Here we perform numerical simulations of the following two cases with L modified: (1) $L = 15$ μm, and (2) $L = 35$ μm. The characteristic times are extracted from the simulations, and the values are (1) $\tau_1 = 218$ μs and $\tau_2 = 20$ μs (the ratio $\tau_1/\tau_2 = 10.9$), and (2) $\tau_1 = 279$ μs and

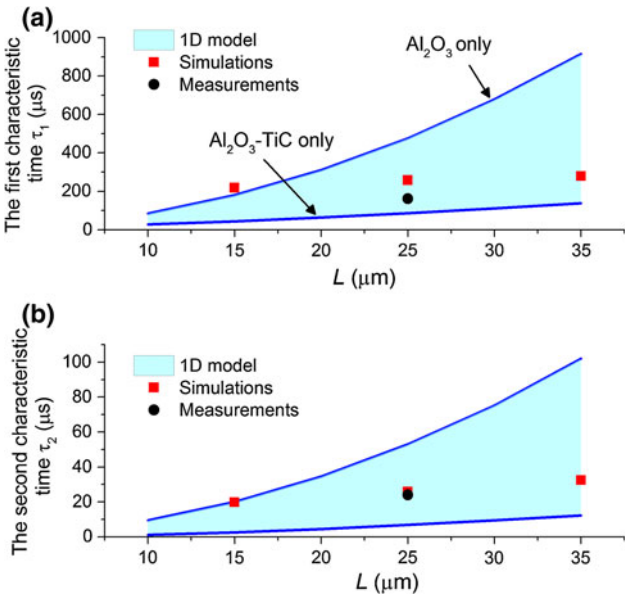

Fig. 7 Overlay of *upper* and *lower* bounds by the 1D model, data points computed by the FEM/air-bearing simulations, and read-back signal measurements for **a** the first characteristic time τ_1 and **b** the second characteristic time τ_2 as a function of L

$\tau_2 = 32$ μs (the ratio $\tau_1/\tau_2 = 8.7$). We plot those along with the values from Eq. (8) and our read-back signal measurements in Fig. 7a, b. The results show that the simple 1D model is efficient to predict the trends and bounds of the first two characteristic times τ_1 and τ_2 of a given design. The ratio of τ_1 to τ_2 is approximately 10 for the analytical, numerical, and experiment results. When the heater is placed closer to the ABS ($L = 15$ μm), the characteristic times calculated by the 1D model made of Al_2O_3 and the FEM/air-bearing simulations coincide, implying that the 1D assumption is valid in this condition. Most of the heat is dissipated to the air bearing through the surrounding overcoat (Al_2O_3) between the heater and the air-bearing surface when L is small. As L increases ($L = 35$ μm), the simulated times also increase at a rate similar to that of the Al_2O_3–TiC case, indicating that in this condition the dominant heat loss is through the slider substrate ($D = 7.38 \times 10^{-6}$ m^2/s) instead of the overcoat ($D = 5.7 \times 10^{-7}$ m^2/s) due to the much larger diffusivity of the substrate material.

4 Conclusion

We have studied the transient characteristics of nanoscale air bearings subjected to Joule heating. Our experimental data and FEM/air-bearing numerical simulations reveal that the transient responses exhibit multiple characteristic times. We present a simple 1D analytical model and identify the nature of the transient characteristics. The model also provides an efficient way to obtain the trends and bounds of a particular design, which is useful when used in complement with the more accurate and time-consuming simulation approach. This model may also explain the much faster response observed in HAMR.

Acknowledgments This work is supported in part by the National Science Council of Taiwan under Contract NSC 101-2221-E-002-151 and NSC 102-2221-E-002-178. I thank Dr. Li Xu of TSMC Solar and Prof. Mei-Jiau Huang of National Taiwan University for helpful discussions.

References

1. Cukier, K., Mayer-Schoenberger, V.: The rise of big data. Foreign Aff. **92**, 28–40 (2013)
2. Marchon, B., Pitchford, T., Hsia, Y., Gangopadhyay, S.: The Head-disk interface roadmap to an areal density of 4 Tbpsi. Adv. Tribol. **2013**, 521086 (2013)
3. Tang, Y., Hong, S., Kim, N., Che, X.: Overview of fly height control applications in perpendicular magnetic recording. IEEE Trans. Magn. **43**, 709–714 (2007)
4. Harker, J.M., Brede, D.W., Pattison, R.E., Santana, G.R., Taft, L.G.: A quarter century of disk file innovation. IBM J. Res. Dev. **25**, 677–690 (1981)
5. Su, L., Hu, Y., Lam, E.L., Li, P., Ng, R.W., Liang, D., Zheng, O., Liu, H., Deng, Z., Zhang, J.: Tribological and dynamic study of head disk interface at sub-1-nm clearance. IEEE Trans. Magn. **47**, 111–116 (2011)
6. Juang, J.-Y., Chen, D., Bogy, D.B.: Alternate air bearing slider designs for areal density of 1 Tb/in 2. IEEE Trans. Magn. **42**, 241–246 (2006)
7. Yeack-Scranton, C.E., Khanna, V.D., Etzold, K.F., Praino, A.P.: An active slider for practical contact recording. IEEE Trans. Magn. **26**, 2478–2483 (1990)
8. Juang, J.-Y., Bogy, D.B.: Nonlinear compensator design for active sliders to suppress head-disk spacing modulation in hard disk drives. IEEE/ASME Trans. Mechatron. **11**, 256–264 (2006)
9. Juang, J.-Y., Bogy, D.B.: Controlled-flying proximity sliders for head-media spacing variation suppression in ultralow. IEEE Trans. Magn. **41**, 3052–3054 (2005)
10. Juang, J.-Y., Ambekar, R.P., Bogy, D.B., Bhatia, C.S.: Fabrication and experimental study of Al_2O_3–TiC sliders with piezoelectric nanoactuators for flying height control. Microsyst. Technol. **13**, 751–757 (2006)
11. Juang, J.-Y., Bogy, D.B., Bhatia, C.S.: Design and dynamics of flying height control slider with piezoelectric nanoactuator in hard disk drives. J. Tribol. **129**, 161 (2007)
12. Juang, J.-Y., Bogy, D.B.: Air-bearing effects on actuated thermal pole-tip protrusion for hard disk drives. J. Tribol. **129**, 570 (2007)
13. Juang, J.-Y., Nakamura, T., Knigge, B., Luo, Y., Hsiao, W.-C., Kuroki, K., Huang, F.-Y., Baumgart, P.: Numerical and experimental analyses of nanometer-scale flying height control of magnetic head with heating element. IEEE Trans. Magn. **44**, 3679–3682 (2008)
14. Juang, J.-Y., Forrest, J., Huang, F.-Y.: Magnetic head protrusion profiles and wear pattern of thermal flying-height control sliders with different heater designs. IEEE Trans. Magn. **47**, 3437–3440 (2011)
15. Wallace, R.L.: The reproduction of magnetically recorded signals. Bell Syst. Tech. J. **30**, 1145–1173 (1951)
16. Boettcher, U., Li, H., De Callafon, R.A., Talke, F.E.: Dynamic flying height adjustment in hard disk drives through feedforward control. IEEE Trans. Magn. **47**, 1823–1829 (2011)
17. Incropera, F.P., DeWitt, D.P., Bergman, T.L., Lavine, A.S.: Foundations of heat transfer. Wiley, London (2013)